*2014 VR&D Users Conference, Experiences in Design Optimization*
*Oct 27-28, 2014 Monterey CA, USA*

# Dynamically Constrained Optimum Trajectory Generation for A Distressed Controlled Aerial System (CAS)

**Nesrin Sarigul-Klijn, Ph.D.**[1]
Mechanical and Aerospace Engineering, University of California Davis, Davis, CA 95616-5294, USA
Email: nsarigulklijn@ucdavis.edu

**Abstract:** The ultimate goal of in-flight trajectory optimization of a controlled aerial system is to safely land with zero casualties and no property damage. The aerial systems could be remotely, autonomously or hybrid controlled, (R-CAS, A-CAS, H-CAS). In-flight trajectory generation task forms a tightly coupled multidisciplinary optimization problem involving aerodynamics, structural dynamics, vehicle health monitoring and guidance-navigation-control as well as human decisions. This paper presents a novel approach in formulating an objective function and incorporating constraints dynamically as more information becomes available. Once the objective function is formulated and dynamic constraints are adapted in real time, proven Design Optimization Tools are employed. Numerical results from optimized trajectories will be included in the paper. It is anticipated that this approach will help reduce pilot (human or auto) workload and provide a contingency plan under an in-flight distress situation.

**Keywords:** Multidisciplinary optimization, Real-time trajectory generation, controlled aerial systems (CAS)

## Table of Contents



## I. Introduction

Flight automation systems and simulators are becoming more sophisticated for usual flight operations, however, there is much work to be done to extend this for unusual or flight under in-flight distressed situations. The current state of the art is to land at the nearest airport. If this were not the case, a minimum distance strategy would dictate an immediate descent and landing wherever the aerial system intersects the ground. Thus the suitability of a given landing site depends on a multitude of factors. Typically, a heuristic approach is used to limit the number of potential landing sites to those that meet a set of standards such as sufficient runway length. A flight plan is then created to land at the nearest of these permissible airports.

While this is mostly an effective simple method, it does have one significant shortcoming: it does not account for any progressive failures. A good example is a fuel leak causing an in-flight distress situation. It is difficult to predict the rate at which fuel will be lost, especially if there is a chance of more leaks, or uncertainty about the reliability of the fuel level sensors. In that case, the predicted range will have high uncertainties. Now consider the airport selection problem where there are multiple airports nearby, with varying facilities. Aircraft over even sparsely populated areas will have a several opportunities for landing, all with varying characteristics such as distance away from the aircraft, maneuvers required to reach the runway, runway length and orientation, fire and emergency crew presence, size and capability, proximity to hospitals and weather conditions. All of these factors contribute to the overall safety of a given flight trajectory. New approaches which will help improve mission success under a distress event must be considered.

The UC Davis Distressed Aircraft Recovery Technique (DART) research group has been working on such a framework. This unique DART architecture has two major departures from the common strategy for dealing with in-flight distress situations. The first is the consideration of all factors of the flight plan, from distress event to successful landing. The







[1] Professor and Director of Space Engineering Research and Graduate Program (SpaceED)
Phone: +1. 530.752.0682

second is prediction and correction of landing site dynamically to account for changes in distressed controlled aerial system (CAS). The mathematical model of DART architecture is a tightly coupled multidisciplinary optimization involving aerodynamics, structural dynamics, vehicle health monitoring/diagnostics and guidance-navigation-control as well as human decisions, (Fig. 1). References (1 through 12) contain specific research findings in more details.

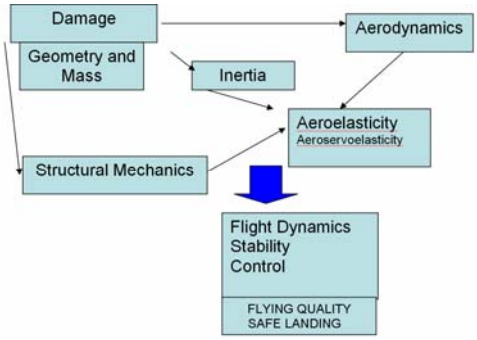


**Fig. 1** Elements of DART architecture prior to Dynamically Constrained Optimization[1-12].

## II. DART Architecture

The aerial systems in distress could be remotely, autonomously or hybrid controlled, (R-CAS, A-CAS, H-CAS). The ultimate goal of in-flight trajectory optimization is to safely land with zero casualties and no property damage. If human controlled, all available landing sites are first evaluated and then the pilot makes a judgment call to which site to attempt to land at, and how best to get there. Our DART architecture attempts to take that process and automates it, introducing more mathematical formalism thereby making all pilots (human or auto) regardless of their experience levels to find the most suitable site.

The mission phases for a distressed CAS are divided as follows:

**Phase.1 Enroute-Flight/Approach to Land:**

This encompasses the time from the distress event until the aerial system reaches the landing-site environment. One of the contributors to further failure is duration in the air. The longer the airborne duration is, the more likely something else will fail. Further maneuvers, weather, issues with progressive structural damage and control failures, among others, also contribute.

**Phase.2 Touchdown/Rollout/Stop:**

This covers from the time the aircraft touches the runway until it comes to a complete stop. At this point, failure is a function of runway environment and approach speed. Specifically, the area beyond the runway is important in the event that the aircraft cannot slow within the length of the runway or overshoots the desired touchdown location.

**Phase.3 Evacuation/Rescue:**

This covers from the time that the aircraft stops until the entire injured are in a hospital. The primary issue here is the proximity of fire crews, ambulances and hospitals.

There are many challenges to real time dynamic trajectory generation just after a distressed condition. In our DART architecture, controlled aerial system dynamic equations are first derived and dynamic objective function is formulated which will maximize safe outcome with case specific *"optimization field variables"* which includes flyable trajectory elements under current distress induced control and strength constraints. Augmented functional is first obtained using Lagrange multipliers. Details of the optimization and its numerical solution are presented in Section III.

Without loss of generality of DART architecture, which deals with in flight distress situations, in this paper an in-flight primary wing structure damaged transport aircraft formulations are derived and used in the general multidisciplinary optimization formulated. In the recent years there has been many in flight wing damage incidents to aircraft, a few such in-flight damaged aircraft are depicted from open literature in Fig. 2. (left) MANPADS, and (right) mid-air collision induced damage.

**Fig. 2** In-flight damaged A-300-600 aircraft (left) and F-15 aircraft starboard wing damage due to mid-air.

**A. Damaged Aircraft Dynamic Equations**

The equations of motion for an asymmetrically damaged aircraft will be presented here. The equations will be expressed in terms of a body-fixed axis whose origin is not the center of gravity. A Lagrangian approach is used to derive the equations of motion. Only the kinetic energy of the aircraft will be considered initially, the aerodynamic and gravitational forces and moments will be added later as applied forces and moments since they are more easily defined.

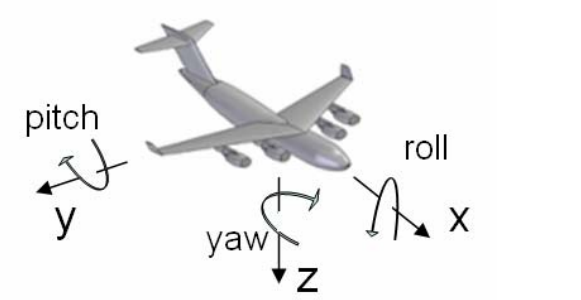


**Fig. 3** Body fixed coordinates and pitch, roll, yaw control.

The total kinetic energy, $T$, of a rigid aircraft is expressed in equation below.

$$T = \frac{1}{2}\int \overline{V}^T \overline{V} dm$$
$$= \frac{1}{2}\int \left(V + \tilde{r}^T \omega\right)^T \left(V + \tilde{r}^T \omega\right) dm = \frac{1}{2}\int \left(V^T V + 2V^T \tilde{r}^T \omega + \omega^T \tilde{r}\tilde{r}^T \omega\right) dm \tag{1}$$

As a matter of convention, the cross product of two vectors, $\omega$ and $r$, will be noted as follows:

$$\omega \times r = \tilde{r}^T \omega$$
$$= \begin{bmatrix} 0 & -r_3 & r_2 \\ r_3 & 0 & -r_1 \\ -r_2 & r_1 & 0 \end{bmatrix}^T \begin{bmatrix} \omega_1 \\ \omega_2 \\ \omega_3 \end{bmatrix} = \tilde{\omega} r = \begin{bmatrix} 0 & -\omega_3 & \omega_2 \\ \omega_3 & 0 & -\omega_1 \\ -\omega_2 & \omega_1 & 0 \end{bmatrix} \begin{bmatrix} r_1 \\ r_2 \\ r_3 \end{bmatrix} \tag{2}$$

The mass properties are expressed in equation (3), where $M$ is the scalar mass of the body multiplied by the identity matrix, $S$ is the first moment of inertia which is normally *"zero"* for undamaged aircraft, and $I$ is the second moment of inertia. The translational velocity vector and the angular velocity vector are also enumerated in equation (3).

$$M = \int dm \quad \tilde{S} = \int \tilde{r} dm \quad I = \int \tilde{r}\tilde{r}^T dm$$
$$V = \begin{bmatrix} u & v & w \end{bmatrix}^T \quad \omega = \begin{bmatrix} p & q & r \end{bmatrix}^T \quad S = \begin{bmatrix} S_x & S_y & S_z \end{bmatrix}^T \tag{3}$$

Using the terms from equation (3), the kinetic energy of the body is expressed in equation (4).

$$T = \frac{1}{2}\left(MV^T V + 2V^T \tilde{S}^T \omega + \omega^T I \omega\right) \tag{4}$$

Taking the derivative of the kinetic energy with respect to the velocity vector, $V$, and the angular velocity vector , $\omega$ , yields the following expression in equation (5).

$$\frac{\partial T}{\partial V} = MV + \tilde{S}^T \omega$$
$$\frac{\partial T}{\partial \omega} = \tilde{S} V + I\omega \tag{5}$$

To arrive at the equations of motion, the kinetic energy relation to generalized forces and moments is taken in equation

$$\partial/\partial t\left(\frac{\partial T}{\partial V}\right) + \tilde{\omega}\frac{\partial T}{\partial V} = \vec{F}_{gravity} + \sum \vec{F}_{aero}$$

$$\partial/\partial t\left(\frac{\partial T}{\partial \omega}\right) + \tilde{V}\frac{\partial T}{\partial \omega} + \tilde{\omega}\frac{\partial T}{\partial \omega} = \vec{M}_{gravity} + \sum \vec{M}_{aero} \tag{6}$$

After combining equations (5) and (6) together and expanding all terms, the equations of motion becomes as listed in equation (7).

$$\begin{aligned}
&m(\dot{u} - rv + qw) + S_z\dot{q} - S_y\dot{r} + S_z pr + S_y pq - S_x q^2 - S_x r^2 \\
&= X_{gravity} + \sum X_{aero} \\
&m(\dot{v} + ru - pw) - S_z\dot{p} + S_x\dot{r} + S_z qr + S_x pq - S_y p^2 - S_y r^2 \\
&= Y_{gravity} + \sum Y_{aero} \\
&m(\dot{w} + pv - qu) + S_y\dot{p} - S_x\dot{q} + S_x pr + S_y qr - S_z p^2 - S_z q^2 \\
&= Z_{gravity} + \sum Z_{aero} \\
&I_{xx}\dot{p} - I_{xy}\dot{q} - I_{xz}\dot{r} + I_{xy} pr - I_{xz} pq + \left(I_{zz} - I_{yy}\right)qr + I_{yz}\left(r^2 - q^2\right) \\
&- S_z\left(\dot{v} + ru - pw\right) + S_y\left(\dot{w} + pv - qu\right) = L_{gravity} + \sum L_{aero} \\
&- I_{xy}\dot{p} + I_{yy}\dot{q} - I_{yz}\dot{r} + I_{yz} pq - I_{xy} qr + \left(I_{xx} - I_{zz}\right)pr + I_{xz}\left(p^2 - r^2\right) \\
&+ S_z\left(\dot{u} + qw - rv\right) - S_x\left(\dot{w} + pv - qu\right) = M_{gravity} + \sum M_{aero} \\
&- I_{xz}\dot{p} - I_{yz}\dot{q} + I_{zz}\dot{r} + I_{xz} qr - I_{yz} pr + \left(I_{yy} - I_{xx}\right)pq + I_{xy}\left(q^2 - p^2\right) \\
&+ S_x\left(\dot{v} + ru - pw\right) - S_y\left(\dot{u} + qw - rv\right) = N_{gravity} + \sum N_{aero}
\end{aligned} \tag{7}$$

These are the descriptions of how the forces and moments on the aircraft are related to a fixed axes system attached to the aircraft body. However, the effective force of gravity in the body fixed axes system is dependent on the orientation of the body fixed axis system with respect to the Earth-centered-inertial (ECI) fixed frame, Fig 4.

There is a transformation between the two

coordinate frames that can be expressed as a matrix transformation.

$$\mathbf{x}_b = \mathbf{\Gamma}^{-1}\mathbf{x}_f \tag{8}$$

The transformation matrix $\mathbf{\Gamma}^{-1}$ can be represented as three ordered rotations. $\psi$ is the angle rotation about the fixed system z-axis. $\theta$ is the angle rotation about the new system y-axis to bring the x-axis in line with the body fixed x-axis. $\phi$ is the angle rotation about the body fixed x-axis to bring the y-axis and z-axis in line with the body fixed y-axis and z-axis. $\psi$, $\theta$, and $\phi$ are called the yaw, pitch, and roll angles and are referred to as the Euler angles. The order of rotation is performed with yaw first, pitch second, and roll last. The system of equations is known as the set of kinematics equations. The next transformation will be for gravity. The force of gravity in the inertial frame is a force vector along the z-axis. This same force in the body fixed axis system can be found using the transformation matrix in equation (9). Where "c" is cosine and "s" is sine.

$$\Gamma^{-1} = \begin{bmatrix} c\theta c\psi & c\theta s\psi & -s\theta \\ (-c\phi s\psi + s\phi s\theta c\psi) & (c\phi c\psi + s\phi s\theta s\psi) & s\phi c\theta \\ (s\phi s\psi + c\phi s\theta c\psi) & (-s\phi c\psi + c\phi s\theta s\psi) & c\phi c\theta \end{bmatrix} \tag{9}$$

Using equation (10) and the Earth induced gravity vector, we can enumerate the gravitational forces in the aircraft's body fixed frame of reference.

$$\vec{F}_{gravity} = \begin{bmatrix} X_{gravity} \\ Y_{gravity} \\ Z_{gravity} \end{bmatrix} = \Gamma^{-1}\begin{bmatrix} 0 \\ 0 \\ mg \end{bmatrix} = \begin{bmatrix} -mgs\theta \\ mgs\phi c\theta \\ mgc\phi c\theta \end{bmatrix} \tag{10}$$

Given the gravitational force in the body-fixed frame, the moment caused by center of gravity shift is calculated.

$$\vec{M}_{gravity} = \begin{bmatrix} L_{gravity} \\ M_{gravity} \\ N_{gravity} \end{bmatrix} = \frac{1}{m}\tilde{S}\begin{bmatrix} X_{gravity} \\ Y_{gravity} \\ Z_{gravity} \end{bmatrix} = \begin{bmatrix} S_y gc\theta c\phi - S_z gc\theta s\phi \\ -S_x gc\theta c\phi - S_z gs\theta \\ S_y gs\theta + S_x gc\theta s\phi \end{bmatrix} \tag{11}$$

The kinematics equations can be decoupled from the rest of the system because there are no relations that depend on the velocity in the fixed inertial frame. This results in nine unknown dependent variables ($u$, $v$, $w$, $p$, $q$, $r$, $\phi$, $\theta$, $\psi$) and only six equations available. The last three equations to form a closed system involve the relationship between the rate of rotation of the aircraft and the time rate of change of the Euler angles. After usual derivations the rates of rotation in the body fixed axis system can be expressed in terms of the time rates of change of the Euler angles.

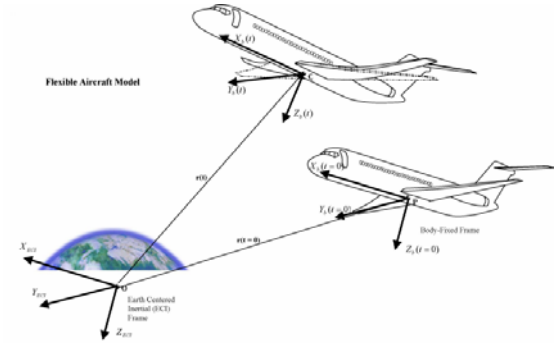


**Fig. 4** Earth-centered-inertial (ECI) coordinates and body fixed initial and final coordinates.

$$\begin{Bmatrix} p \\ q \\ r \end{Bmatrix} = \begin{bmatrix} 1 & 0 & -s\theta \\ 0 & c\phi & s\phi c\theta \\ 0 & -s\phi & c\phi c\theta \end{bmatrix}\begin{Bmatrix} \dot{\phi} \\ \dot{\theta} \\ \dot{\psi} \end{Bmatrix} \tag{12}$$

The matrix can be inverted to write the Euler rates in terms of the body rotation.

$$\begin{Bmatrix} \dot{\phi} \\ \dot{\theta} \\ \dot{\psi} \end{Bmatrix} = \begin{bmatrix} 1 & s\phi\tan\theta & c\phi\tan\theta \\ 0 & c\phi & -s\phi \\ 0 & s\phi\sec\theta & c\phi\sec\theta \end{bmatrix}\begin{Bmatrix} p \\ q \\ r \end{Bmatrix} \tag{13}$$

Linearization about the reference values ($v_0 = w_0 = p_0 = q_0 = r_0 = 0$) yields the linearized equations of motion (Eqs. 15). It is assumed that the *x-axis* is aligned with the direction of forward motion of the aircraft, and those reference values will be zero. Later, we will assume that the *x-axis* is aligned with a "wind axis", (Figure 5).

$$\begin{aligned}
&m\Delta\dot{u} + S_z\Delta\dot{q} - S_y\Delta\dot{r} = -mgc\theta_0\Delta\theta + \sum X_{aero} \\
&m(\Delta\dot{v} + u_0\Delta r) - S_z\Delta\dot{p} + S_x\Delta\dot{r} = -mgs\theta_0 s\phi_0\Delta\theta + mgc\theta_0 c\phi_0\Delta\phi + \sum Y_{aero} \\
&m(\Delta\dot{w} - u_0\Delta q) + S_y\Delta\dot{p} - S_x\Delta\dot{q} = -mgs\theta_0 c\phi_0\Delta\theta - mgc\theta_0 s\phi_0\Delta\phi + \sum Z_{aero} \\
&I_{xx}\Delta\dot{p} - I_{xy}\Delta\dot{q} - I_{xz}\Delta\dot{r} - S_z(\dot{v} + \Delta r u_0) + S_y(\dot{w} - \Delta q u_o) = \\
&(S_z gs\theta_o s\phi_o - S_y gs\theta_o c\phi_o)\Delta\theta - (S_y gc\theta_o s\phi_o + S_z gc\theta_o c\phi_o)\Delta\phi + \sum L_{aero} \\
&-I_{xy}\dot{p} + I_{yy}\dot{q} - I_{yz}\dot{r} + S_z(\dot{u}) - S_x(\dot{w} - \Delta q u_o) = \\
&(S_x gs\theta_o c\phi_o - S_z gc\theta_o)\Delta\theta + (S_x gc\theta_o s\phi_o)\Delta\phi + \sum M_{aero} \\
&-I_{xz}\dot{p} - I_{yz}\dot{q} + I_{zz}\dot{r} + S_x(\dot{v} + \Delta r u_0) - S_y(\dot{u}) = \\
&(S_y gc\theta_o - S_x gs\theta_o s\phi_o)\Delta\theta + (S_x gc\theta_o c\phi_o)\Delta\phi + \sum N_{aero}
\end{aligned} \tag{14}$$

By dividing the state space into two pieces

$$x=\begin{bmatrix}\Delta u\\ \Delta v\\ \Delta w\\ \Delta p\\ \Delta q\\ \Delta r\\ \Delta\theta\\ \Delta\phi\end{bmatrix} x_1=\begin{bmatrix}\Delta u\\ \Delta v\\ \Delta w\\ \Delta p\\ \Delta q\\ \Delta r\end{bmatrix}, x_2=\begin{bmatrix}\Delta\theta\\ \Delta\phi\end{bmatrix}, x=\begin{bmatrix}x_1\\ x_2\end{bmatrix} \tag{15}$$

We will reorganize linearized equations derived above in the form listed below. The individual sub-matrices are defined in (Table A1, in Appendix).

$$\dot{x}=\begin{bmatrix}(E-T)^{-1}\Theta_1 & (E-T)^{-1}\Theta_2\\ \Omega & 0_{2x2}\end{bmatrix}x + \begin{bmatrix}(E-T)^{-1}\Xi & 0_{6x2}\\ 0_{2x6} & 0_{2x2}\end{bmatrix}x+\begin{bmatrix}(E-T)^{-1}\Psi\\ 0_{2xm}\end{bmatrix}\delta \tag{16}$$

The equations are shown in the following order force equations, moment equations, and the Euler angle relation to the body fixed axis system.

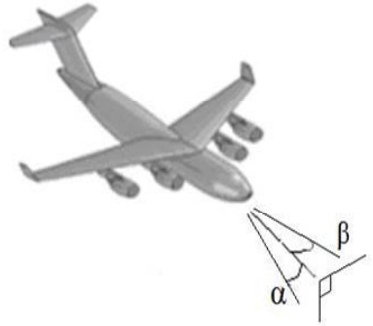


**Fig. 5** Body fixed Wind axis system, angle of attack and side-slip angle.

**Wind Axes Rotation.** The linearized equations in the previous section relied upon the assumption that the *x-axis* was in the same direction as the direction of the forward velocity of the aircraft. Thus, the point about which the linearization was done was at $v_0 = w_0 = p_0 = q_0 = r_0 = 0$ . It is uncommon for an aircraft to be trimmed at zero angle of attack and it is more common for the aircraft to have its nose tilted slightly up during steady level flight.

In general, $w_0$ value is not zero in the body coordinates. Hence, the body axes are rotated so that $w_0$ really is zero at equilibrium, the stability axes system convention. If the aircraft is trimmed in a sideslip condition, the axes are first rotated with the angle of attack and then rotated to the correct sideslip angle. The only necessary update to the equations of motion is to change the mass properties to accommodate this rotation to the wind axes. The changes are listed below (Table A3) in Appendix.

**B. Damaged Aircraft Aerodynamics**

High fidelity and reduced order methods both are used. Time-dependent compressible Navier-Stokes equations are solved to generate known damage conditions to obtain a database using the two-equation Shear Stress Transport (*SST*) model. In-flight scenario specific adjustments are conducted using reduced order models and coupled in Vehicle Monitoring and Diagnostics.

**C. Adaptive System Identification/Vehicle Health Monitoring and Diagnostics**

The cyclic nature of flight loads causes ageing of aerial systems[1] Therefore, it is necessary to take deterioration into account when performing structural damage assessment of in-flight systems. Most methods focus on looking for damage using one set of data from the undamaged and damaged states. Treating the problem in this fashion ignores the real-time and long-duration of continuous monitoring a structure so that gradual degradation and damage from severe events, such as impacts, can be detected. Adaptive recognition of aerial vehicle health is required in order provide better estimate of spontaneous damage events [3-7].

By adding a System Identification into the flight management system, we can determine the system performance in real time, ensuring a feasible flight path. By integrating a structural health monitoring system, the structural loads on the airframe can be optimized as well. Most of the available damage assessment techniques are

capable of detecting damage, location and/or severity; however, none of the available techniques provide an approach that can take into account structural deterioration due to ageing overtime in the parameter estimation and results classification levels. In order to address the uncertainty in estimating system parameters due to structural deterioration, our team developed a modified exponential forgetting and resetting algorithm (MEFRA) for adaptive system identification to spontaneous damage of structures using vibration measurements. The modal and time series parameters are to be identified using measured structural response from an undamaged system and then from a damaged system. Once the model structure is chosen or given, the problem of system identification is reduced to the problem of adaptive parameter estimation and tracking. Individual and combined binary classification techniques are utilized to search for the most probable class of event by comparing the relative probabilities for impact damages.

Due to the uncertainties[5] involved in obtaining robust and reliable damage assessment estimates, system identification and pattern recognition techniques will be used properly categorize spontaneous damage events in deteriorating structures. Given that structural deterioration is well tracked, vibration-based feature extraction and classification will be performed to estimate spontaneous damage. Multiple dimensionality reduction and classification techniques applied to vibration-based data will be evaluated and compared. Once potential damages have been detected, changes in modal parameters between the prior structural response and current damaged structure response are analyzed via the damage index method.

Dimensionality reduction and feature classification methods were employed to discriminate between damaged and undamaged data. A comparative study was conducted of dimensionality reduction and classification techniques. From the results obtained, we may conclude that statistical discrimination of damage from undamaged data is more dependent on the efficiency of the dimensionality reduction method, than the classification method.

In house experimental data from simulated damage cases at our Transportation Noise Control Center's, TNCC anechoic chamber is also collected and vibration/acoustic/optical based techniques are under investigation together with high fidelity FEA (Fig A1 in Appendix) and reduced order simulations [7-12].

## III. Dynamically Constrained Optimization

### A. Formulation

In-flight trajectory generation task forms a tightly coupled multidisciplinary optimization problem involving aerodynamics, structural dynamics, vehicle health monitoring and guidance-navigation-control as well as human decisions. This research involves a novel approach[1] in formulating an objective function and incorporating constraints dynamically as more information becomes available (Figure 6, Table 3).

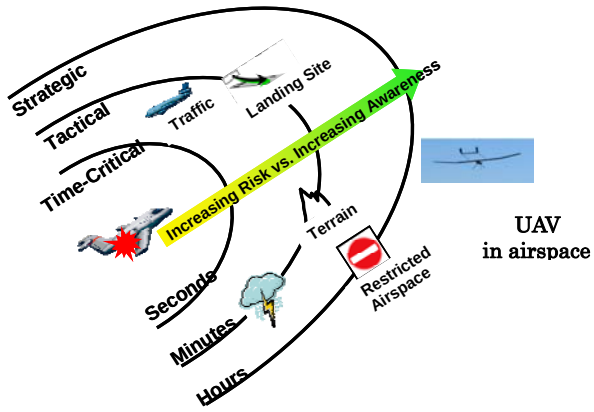


**Fig. 6** Distressed aircraft event time scales. Seconds, minutes, hours and integration of new information dynamically in optimnization.

Two types of objective functions are formulated: 1) Expected path length after distress even until landing and 2)Probability of mission success under dynamic conditions. The constraint equations are formulated for distress event specifically and updated dynamically as new information become available, Table 3. "*Optimization field variables*" are identified for each distress scenario and it does at least include some control parameters. Control constrains are usually placed as "limits" on *optimization field variables.*

The final form of the objective function is formulated using Augmented Lagrange

Multipliers Method. In equation (18) the $\Lambda_s$ are the Lagrange multipliers, E is the objective function; $E^a$ is the augmented objective function. The augmented functional for the optimization become, symbolically:

$$Ea = E + \Lambda_1 g(s) + \Lambda_2 h(s) \qquad (18)$$

**Table 3.** Trajectory prediction, conflict and resolution for en-route phase.

| | Information Accuracy | Principle | Trajectory | Conflict | Maneuver Priority |
|---|---|---|---|---|---|
| Short-Term < 10mins | Precise | Separation Assurance | Optimization and Execution | Immediate action, accurate state and | Distress Event: other aircraft will be informed |
| Medium-Term < 30mins | Stochastic | Traffic | Prediction | Timely actions, detection and mitigation | Off-nominal -according to situation, recovery |
| Long-Term > 30mins | Stochastic and Imprecise | Flow Management | Flexibility - Plan | Trajectory management, A-CAS avoidance | Nominal |

The resultant equations are solved using numerical optimization techniques and will be briefly explained. The reader will be referred to an excellent book by Vanderplaats for further details in numerical optimization[13].

### B. Solution: Numerical Optimization

Once the objective function is formulated (Equation 18) and dynamic constraints are adapted in real time, numerical optimization is employed using 2 different approaches:

**Approach 1)** An in house developed variable metric algorithm within our DART architecture software. This choice was made owing to prior good experience of the author with the algorithm BFGS (Broydon-Fletcher-Goldfarb-Shanno). This algorithm carries forward the history from previous iterations and is likely to yield with more reliable results than other algorithms however at the expense of some computational cost. BFGS worked very well for the test cases. In order to increase efficiency we needed to investigate other algorithms. Therefore we also tried Approach 2.

**Approach 2)** Use of proven DOT: Design Optimization Tools (VR&D, Inc.) by calling from our main program. Since DOT is well tested and also contains many different algorithms it helped reduce research time in our search for an efficient and reliable numerical solution algorithm. For our multidisciplinary optimization mathematical form, Fletcher-Reeves conjugate direction, a first order method worked the best. The Fetcher-Reeves method is to theoretically minimize a quadratic function in n or fewer iteration cycles[13]. However, in practice it does take a few restarts due to non-quadratic nature of the multidisciplinary optimization problem in hand. This first order method Fletcher-Reeves from DOT has been identified as the most efficient one in our applications so far. Next section gives example results from a case study.

### C. Case Study Results

Our DART architecture together with the numerical optimization solution algorithms was used for a simulated wing damage distress event given below:

A transport category airplane encountered in flight right wing structural damage while on a descent out of flight level 200 (20,000 feet) into San Francisco International Airport (KSFO), as marked in sectional charts above. Indicated airspeed was 340 knots. The distress event occurred while passing north of Stockton airport (KSCT) .

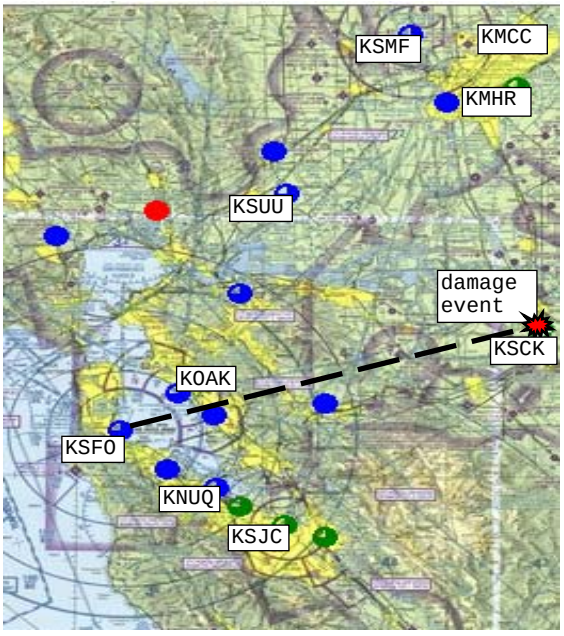


Numerical results from optimized trajectories are provided in figures below. Paths are built from three straight and two circular turn segments with altitude

and velocity profiles. Turn radii, time aloft, and runway length are determined and stored. Under a flight distress condition, distance to the landing site becomes even more important. Hence the novel probabilistic method developed here offers improvement by reducing the expected path length while increasing the probability of safe landing given the occurrence of an abort situation, (Fig. 7).

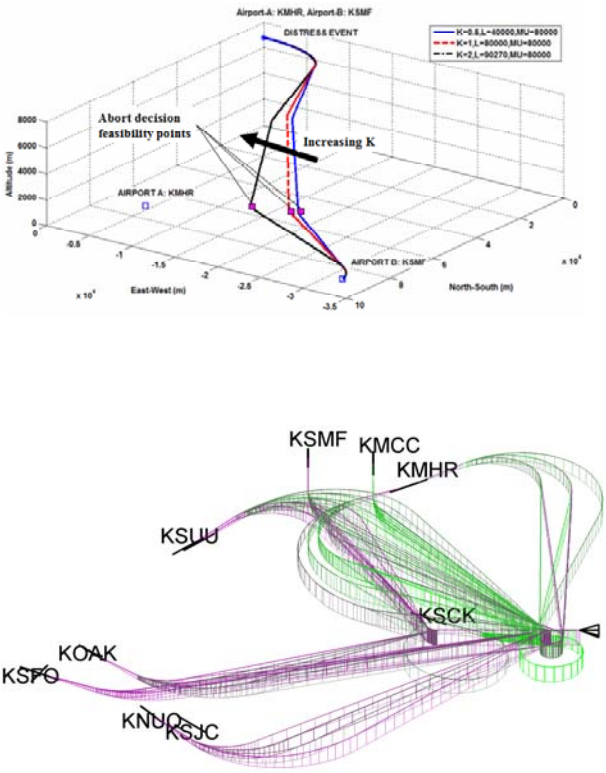


**Fig. 7** Flight paths and effects of parameters on optimum solution.

## Conclusion

The DART architecture was developed and evaluated for several in-flight simulated distress aircraft scenarios. Numerical optimization algorithms evaluated are a variable metric in house development as well as many available algorithms from proven DOT from VR&D, Inc. It is seen that use of Design Optimization Tools allowed rapid selection and evaluation of suitable algorithms for our multidisciplinary newly formulated optimization objective function.

## References


[1] Nesrin Sarigul-Klijn and A. White, "Novel Probabilistic Dynamic Safety Metric Formulations for Flight path determination", *Proceedings of the Institution of Mechanical Engineers, Part G: J. of Aerospace Engineering, 0954410011426516, January 9, (2012).*

[2] Nesrin Sarigul-Klijn "Aeronautical and Space Engineering Materials", In CRC Engineering Handbook (Eds. Dorf.), 2005, Chapter 196, pp 1-13, (2005).

[3] Nesrin Sarigul-Klijn, I. Lopez, S-I Baek, B. Kuo, "Smart Monitoring" of Structural Health in Flight Environment,"*(Invited Keynote) ICEE 2008 Hiroshima, Japan, Oct 9 2008. Proc, of International Conf,* Higashi-Hiroshima, Japan, (2008).

[4] N. Sarigul-Klijn, I. Lopez, M. Sarigul-Klijn, and D. Karnopp, "Vibration Mitigation Using Passive Active Tunable (PAT) System: Experimental Aspects", Journal of Vibration and Acoustics, Volume 129, Issue 2, pp. 209-216, April (2007).

[5] I. Lopez and Nesrin Sarigul-Klijn, "A review of uncertainty in flight vehicle structural damage monitoring, diagnosis and control: Challenges and opportunities" ,*Progress in Aerospace Sciences, Volume 46, Issue 7, October 2010, Pages 247-273, (2010).*

[6] A. Ward and Nesrin Sarigul-Klijn, "Improving Vibration Based damage detection using optical measurements", Proc. of the 2011 ASME Int. Mech. Eng.&,Congress & Exposition, IMECE2011-60330, Nov. 11-17, 2011, Denver, Colorado, USA

[7] I. Lopez and Nesrin Sarigul-Klijn, "Distance similarity matrix using ensemble of dimensional data reduction techniques: Vibration and Aeroacoustics case studies," *Journal of Mechanical Systems and Signal Processing, Volume 23, Issue 7,* October 2009, 2287-2300, (2009).

[8] J. Kim and N. Sarigul-Klijn, "Material/Geometry Adaptive Shape Functions for Rayleight-Ritz Vibration Analysis of Composite Plates", , *Journal of Aircraft,* V. 38, N. 3, 560-564, May-June (2000).

[9] I. Lopez and Nesrin Sarigul-Klijn, "A novel dimensional reduction approach for structural damage diagnosis using feature similarity", In: Health Monitoring of Structural and Biological Systems. Ed: Kundu. Proc. of the SPIE, Vol. 7295 (2009), pp. 72951M-72951M-12 American Institute of Physics, (2009).

[10] B.C. Kuo and Nesrin Sarigul-Klijn, "Three Dimensional CFD Analysis of Micro-tab in Airframe Noise Reduction," AIAA-2008-2864, *Proc of 14th AIAA/CEAS Aeroacoustics Conference (29th AIAA Aeroacoustics Conference),* Vancouver, British Columbia, May 5-7, (2008).

[11] I. Lopez and Nesrin Sarigul-Klijn, "System Identification and Damage Assessment of Deteriorating Hysteretic Structures", AIAA-2008-1738 49th AIAA/ASME/ASCE/AHS/ASC Structures, Structural Dynamics, and Materials Conference 16th

AIAA/ASME/AHS Adaptive Structures Conference, 10t, Schaumburg, IL, Apr. 7-10, (2008)

[12] Kuo, B. and Nesrin Sarigul-Klijn, "Numerical Investigation of Micro-Tab in Airframe Noise", 13th AIAA Aeroacoustic Conference, 2007.

[13] Vanderplaats, G.N., *Numerical Optimization Techniques for Engineering Design*, VR&D, Inc., (1999).

## About the author:

Dr. Nesrin Sarigul-Klijn is a Full Professor of Mechanical and Aerospace Engineering and the Founding Director of Space Engineering Research and Graduate Program, SpaceED at University of California Davis. She received her PhD degree from The University of Arizona. She is also an instrument rated commercial pilot and has piloted 37 different types of aircraft. Her current research activities include fundamental research in distressed aircraft dynamics and controls constraint recovery trajectory optimization, air launching space vehicles, dynamic separation, acoustics, vibrations, flow-structure interactions, and flight testing in her *DynaaTECC* (Dynamics, Acoustics, Aeroelasticity, Theory, Experiments, Computations and Controls) *research group*. Professor Sarigul-Klijn and her graduate students received *the Derek George Astridge Safety in Aerospace Medal of United Kingdom's Institution of Mechanical Engineers* in 2014 for their Distress Aircraft Recovery Technique Research. Dr. Sarigul-Klijn's professional activities include editorial board membership in Progress in Aerospace Journal.

## Nomenclature

| | |
|---|---|
| DART | Distressed Aerial-System Recovery Technique |
| S_J | Path position coincident with J |
| s | Position on the path |
| P(s) | Probability density function for an abort at s |
| E | Expected path length |
| k, λ | Weibull distribution parameter, failure rate, size |

## APPENDIX.

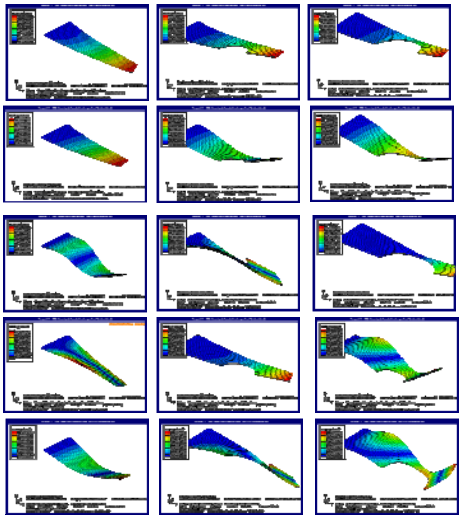

**Fig. A1** Mode shapes of a simulated Damaged wing ( Finite Element Method).

**Table A1.** Linearized State Space representation of damaged aircraft

$$E=\begin{bmatrix} m & 0 & 0 & 0 & S_z & -S_y \\ 0 & m & 0 & -S_z & 0 & S_x \\ 0 & 0 & m & S_y & -S_x & 0 \\ 0 & -S_z & S_y & I_{xx} & -I_{xy} & -I_{xz} \\ S_z & 0 & -S_x & -I_{xy} & I_{yy} & -I_{yz} \\ -S_y & S_x & 0 & -I_{xz} & -I_{yz} & I_{zz} \end{bmatrix}$$

$$\Psi=\begin{bmatrix} \frac{\partial X}{\partial \delta_1} & \cdots & \frac{\partial X}{\partial \delta_m} \\ \vdots & \ddots & \vdots \\ \frac{\partial N}{\partial \delta_1} & \cdots & \frac{\partial N}{\partial \delta_m} \end{bmatrix}$$

$$\Theta_1=\begin{bmatrix} 0 & 0 & 0 & 0 & 0 & 0 \\ 0 & 0 & 0 & 0 & 0 & -mu_0 \\ 0 & 0 & 0 & 0 & mu_0 & 0 \\ 0 & 0 & 0 & 0 & S_y u_0 & S_z u_0 \\ 0 & 0 & 0 & 0 & -S_x u_0 & 0 \\ 0 & 0 & 0 & 0 & 0 & -S_x u_0 \end{bmatrix}$$

$$\Theta_2=\begin{bmatrix} -mgc\theta_0 & 0 \\ -mgs\theta_0 s\phi_0 & mgc\theta_0 c\phi_0 \\ -mgs\theta_0 c\phi_0 & -mgc\theta_0 s\phi_0 \\ g\left(-S_y s\theta_0 c\phi_0 + S_z s\theta_0 s\phi_0\right) & g\left(-S_y c\theta_0 s\phi_0 - S_z c\theta_0 c\phi_0\right) \\ g\left(-S_z c\theta_0 + S_x s\theta_0 c\phi_0\right) & g\left(S_x c\theta_0 s\phi_0\right) \\ g\left(S_y c\theta_0 - S_x s\theta_0 s\phi_0\right) & g\left(S_x c\theta_0 c\phi_0\right) \end{bmatrix}$$

$$\Xi=\begin{bmatrix} \frac{\partial X}{\partial u} & \frac{\partial X}{\partial v} & \frac{\partial X}{\partial w} & \frac{\partial X}{\partial p} & \frac{\partial X}{\partial q} & \frac{\partial X}{\partial r} \\ \frac{\partial Y}{\partial u} & \frac{\partial Y}{\partial v} & \frac{\partial Y}{\partial w} & \frac{\partial Y}{\partial p} & \frac{\partial Y}{\partial q} & \frac{\partial Y}{\partial r} \\ \frac{\partial Z}{\partial u} & \frac{\partial Z}{\partial v} & \frac{\partial Z}{\partial w} & \frac{\partial Z}{\partial p} & \frac{\partial Z}{\partial q} & \frac{\partial Z}{\partial r} \\ \frac{\partial L}{\partial u} & \frac{\partial L}{\partial v} & \frac{\partial L}{\partial w} & \frac{\partial L}{\partial p} & \frac{\partial L}{\partial q} & \frac{\partial L}{\partial r} \\ \frac{\partial M}{\partial u} & \frac{\partial M}{\partial v} & \frac{\partial M}{\partial w} & \frac{\partial M}{\partial p} & \frac{\partial M}{\partial q} & \frac{\partial M}{\partial r} \\ \frac{\partial N}{\partial u} & \frac{\partial N}{\partial v} & \frac{\partial N}{\partial w} & \frac{\partial N}{\partial p} & \frac{\partial N}{\partial q} & \frac{\partial N}{\partial r} \end{bmatrix}$$

$$T=\begin{bmatrix} \frac{\partial X}{\partial \dot{u}} & \frac{\partial X}{\partial \dot{v}} & \frac{\partial X}{\partial \dot{w}} & \frac{\partial X}{\partial \dot{p}} & \frac{\partial X}{\partial \dot{q}} & \frac{\partial X}{\partial \dot{r}} \\ \frac{\partial Y}{\partial \dot{u}} & \frac{\partial Y}{\partial \dot{v}} & \frac{\partial Y}{\partial \dot{w}} & \frac{\partial Y}{\partial \dot{p}} & \frac{\partial Y}{\partial \dot{q}} & \frac{\partial Y}{\partial \dot{r}} \\ \frac{\partial Z}{\partial \dot{u}} & \frac{\partial Z}{\partial \dot{v}} & \frac{\partial Z}{\partial \dot{w}} & \frac{\partial Z}{\partial \dot{p}} & \frac{\partial Z}{\partial \dot{q}} & \frac{\partial Z}{\partial \dot{r}} \\ \frac{\partial L}{\partial \dot{u}} & \frac{\partial L}{\partial \dot{v}} & \frac{\partial L}{\partial \dot{w}} & \frac{\partial L}{\partial \dot{p}} & \frac{\partial L}{\partial \dot{q}} & \frac{\partial L}{\partial \dot{r}} \\ \frac{\partial M}{\partial \dot{u}} & \frac{\partial M}{\partial \dot{v}} & \frac{\partial M}{\partial \dot{w}} & \frac{\partial M}{\partial \dot{p}} & \frac{\partial M}{\partial \dot{q}} & \frac{\partial M}{\partial \dot{r}} \\ \frac{\partial N}{\partial \dot{u}} & \frac{\partial N}{\partial \dot{v}} & \frac{\partial N}{\partial \dot{w}} & \frac{\partial N}{\partial \dot{p}} & \frac{\partial N}{\partial \dot{q}} & \frac{\partial N}{\partial \dot{r}} \end{bmatrix}$$

$$\Omega=\begin{bmatrix} 0 & 0 & 0 & 0 & c\phi_0 & -s\phi_0 \\ 0 & 0 & 0 & 1 & s\phi_0 \tan\theta_0 & c\phi_0 \tan\theta_0 \end{bmatrix}$$

**Table A2**. Wind Axes Transformations

$$C_{w/b} = \begin{bmatrix} c\alpha_0 c\beta_0 & s\beta_0 & s\alpha_0 c\beta_0 \\ -c\alpha_0 s\beta_0 & c\beta_0 & -s\alpha_0 s\beta_0 \\ -s\alpha_0 & 0 & c\alpha_0 \end{bmatrix}$$

$$I_w = C_{w/b}^T I_b C_{w/b} \qquad \vec{S} = \begin{bmatrix} S_x \\ S_y \\ S_z \end{bmatrix}$$

$$\omega = \begin{bmatrix} p \\ q \\ r \end{bmatrix} \qquad \vec{S}_w = C_{w/b}\vec{S}_b$$

$$\vec{V} = \begin{bmatrix} u \\ v \\ w \end{bmatrix} \qquad \omega_w = C_{w/b}\omega_b \qquad \vec{V}_w = C_{w/b}\vec{V}_b$$